Emergent orbital skyrmion lattice in a triangular atom array

Rui Cao,[1] Jinsen Han,[1] Jianmin Yuan,[2,1] Xiaopeng Li,[3,4,5,*] and Yongqiang Li[1,6,†]

[1]*Department of Physics, National University of Defense Technology, Changsha 410073, People's Republic of China*
[2]*Department of Physics, Graduate School of China Academy of Engineering Physics,*
Beijing 100193, People's Republic of China
[3]*State Key Laboratory of Surface Physics, Key Laboratory of Micro and Nano Photonic Structures (MOE),*
and Department of Physics, Fudan University, Shanghai 200433, China
[4]*Institute for Nanoelectronic Devices and Quantum Computing, Fudan University, Shanghai 200433, China*
[5]*Shanghai Qi Zhi Institute, AI Tower, Xuhui District, Shanghai 200232, China*
[6]*Hunan Key Laboratory of Extreme Matter and Applications, National University of Defense Technology,*
Changsha 410073, China

Multiorbital optical lattices have been attracting rapidly growing research interest in the last several years, providing fascinating opportunities for orbital-based quantum simulations. Here, we consider bosonic atoms loaded in the degenerate p-orbital bands of a two-dimensional triangular optical lattice. This system is described by a multiorbital Bose-Hubbard model. We find the confined atoms in this system develop spontaneous orbital polarization, which forms a chiral Skyrmion lattice pattern in a large regime of the phase diagram. This is an orbital version of the skyrmion, reminiscent of those in spin systems. The emergence of the Skyrmion lattice is confirmed in both bosonic dynamical mean-field theory (BDMFT) and exact diagonalization (ED) calculations. By analyzing the quantum-tunneling-induced orbital-exchange interaction in the strong interaction limit, we find the Skyrmion lattice state arises due to the interplay of p-orbital symmetry and the geometric frustration of the triangular lattice. We provide experimental consequences of the orbital Skyrmion state that can be readily tested in cold atom experiments. Our study implies orbital-based quantum simulations could bring exotic scenarios unexpected from their spin analog.

Introduction. The last several years have witnessed rapid progress in preparing atomic multiorbital superfluids in optical lattices [1–10]. Versatile quantum many-body phenomena have been observed by combining multiorbital setting and the complex lattice structure [2,4]. The excited band condensate in a hexagonal lattice has been achieved via a lattice swap technique [2], where a Potts-nematic superfluid appears due to interaction-induced quantum fluctuations. Further cooling of this atomic condensate system [4] leads to a chiral condensate for weakly interacting bosons [11–15]. Universal single-qubit control in the s- and d-orbital subspaces has been implemented with topologically protected robustness [3]. These recent developments open up unprecedented opportunities for orbital-based quantum simulations, by which the realizable quantum many-body states and phenomena could strongly deviate from the spin analog due to the fundamental difference in their symmetry [16].

In this Letter, we study interacting p-orbital bosons in a two-dimensional triangular optical lattice, which corresponds to the experimental setups of hexagonal lattices [2,4] with a large sublattice potential imbalance [17]. Compared to bipartite lattices, such as square or honeycomb lattices, geometric frustrations naturally arise in the triangular lattice, which competes with orbital anisotropy, and can stabilize novel orbital textures. This system is described by a multiorbital Bose-Hubbard model [16,18]. The quantum many-body phases of this system are investigated in the strong interaction regime by bosonic dynamical mean-field theory (BDMFT) and exact diagonalization (ED) calculations. We find an orbital skyrmion lattice state emerges in the Mott insulating regime, which is driven by the interplay of orbital anisotropy and geometric frustration, in the absence of spin-orbit-coupling-induced Dzyaloshinskii-Moriya [19–23] or anisotropic [24,25] interactions, and further-neighbor exchanges [26–29]. The skyrmion lattice state has a composite chirality that spontaneously breaks the time-reversal symmetry. In the orbital setting, two different types of skyrmion lattices occur simultaneously in the degenerate quantum many-body ground states, which is in sharp contrast to the Dzyaloshinskii-Moriya scenario systems [19–23]. Near the Mott-superfluid transition, we find the chiral skyrmion lattice melts to quantum states with stripe and ferroorbital orders.

Model and Hamiltonian. The system of interacting spinless bosonic atoms, loaded into the p-orbital bands of a two-dimensional (2D) triangular optical lattice, can be described

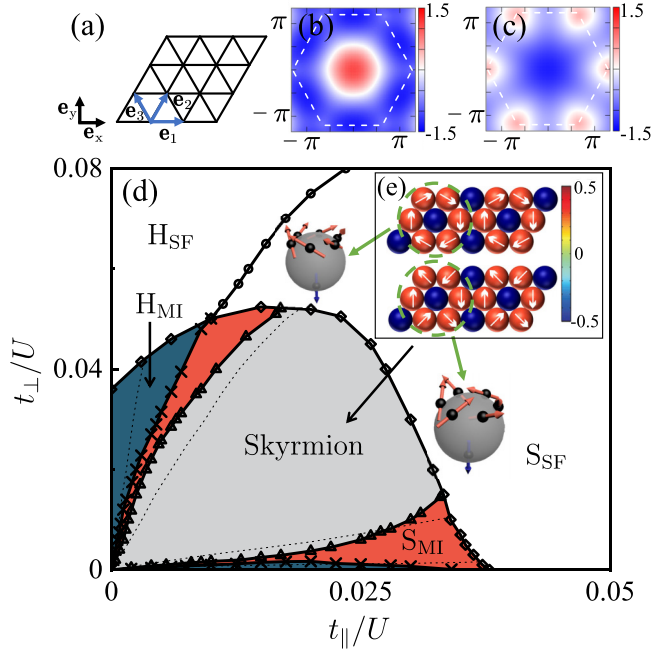*xiaopeng_li@fudan.edu.cn
†li_yq@nudt.edu.cn

FIG. 1. (a) The geometry of the two-dimensional triangular lattice. (b), (c) The energy dispersion of the lowest p-orbital band of a two-dimensional triangular lattice, with (b) $t_\perp = 0$, and (c) $t_\parallel = 0$. (d) Many-body phase diagram in terms of hopping amplitudes $t_\parallel$ and $t_\perp$ for filling $n_\mathbf{r} = 1$, obtained from bosonic dynamical mean-field theory, where the system favors three Mott phases with skyrmion, stripe (S_{MI}), ferroorbital (H_{MI}) textures, and two superfluid phases with stripe (S_{SF}) and ferroorbital (H_{SF}) angular momentum. The dashed lines in Mott insulating are obtained by exact diagonalization. (e) Real-space orbital textures for skyrmion (upper) and anti-skyrmion (down) lattices, where the arrows represent the projection in the xy-plane of orbital polarization texture $\langle \boldsymbol{\mathcal{S}}_\mathbf{r} \rangle$, and the color denotes the z component. The wrapping of the two skyrmion textures is described in the two spheres. The interactions are $U = 3U_1 = 3U_2$.

by a multiorbital Bose-Hubbard model in the tight-binding limit [16,18]

$$
\begin{aligned}
H = {} & t_\parallel \sum_{m,\mathbf{r}} p_{m,\mathbf{r}}^\dagger p_{m,\mathbf{r}+\mathbf{e}_m} - t_\perp \sum_{m,\mathbf{r}} p_{m,\mathbf{r}}'^\dagger p_{m,\mathbf{r}+\mathbf{e}_m}' + \text{H.c.} \\
& + \frac{U}{2} \sum_{\mathbf{r}} n_\mathbf{r}(n_\mathbf{r}-1) + 2U_1 \sum_{\mathbf{r}} n_{x,\mathbf{r}} n_{y,\mathbf{r}} \\
& + \frac{U_2}{2} \sum_{\mathbf{r},\nu\neq\nu'} p_{\nu,\mathbf{r}}^\dagger p_{\nu,\mathbf{r}}^\dagger p_{\nu',\mathbf{r}} p_{\nu',\mathbf{r}} - \mu \sum_{\mathbf{r}} n_\mathbf{r}, \quad (1)
\end{aligned}
$$

where $t_\parallel$ and $t_\perp$ denote the hopping amplitudes between two nearest-neighboring p-orbitals along the parallel and the perpendicular directions, respectively. The lattice annihilation operators $p_{m,\mathbf{r}} \equiv (p_{x,\mathbf{r}}\mathbf{e}_x + p_{y,\mathbf{r}}\mathbf{e}_y) \cdot \mathbf{e}_m$ with the unit vectors $\mathbf{e}_1 = \mathbf{e}_x$ and $\mathbf{e}_{2,3} = \pm\frac{1}{2}\mathbf{e}_x + \frac{\sqrt{3}}{2}\mathbf{e}_y$ for hopping $t_\parallel$ and $p_{m,\mathbf{r}}' \equiv (p_{x,\mathbf{r}}\mathbf{e}_x + p_{y,\mathbf{r}}\mathbf{e}_y) \cdot \mathbf{e}_m'$ with $\mathbf{e}_1' = \mathbf{e}_y$ and $\mathbf{e}_{2,3}' = -\frac{\sqrt{3}}{2}\mathbf{e}_x \pm \frac{1}{2}\mathbf{e}_y$ for hopping $t_\perp$. Here, $\mathbf{e}_m$ is shown in Fig. 1(a) and $p_{x,\mathbf{r}}$ ($p_{y,\mathbf{r}}$) denotes the annihilation operator for the p_x (p_y) orbital degree of freedom at site $\mathbf{r}$. μ is the chemical potential, $n_\mathbf{r} = \sum_\nu p_{\nu,\mathbf{r}}^\dagger p_{\nu,\mathbf{r}}$ with $\nu = x, y$, and U, U_1, and U_2 denote the interaction strengths with $U - 2U_1 = U_2$ as a result of

symmetry analysis for the triangular lattice. In the deep lattice limit, the harmonic approximation of the Wannier function implies $U = 3U_1 = 3U_2$, and consequently the interactions (U and $U_{1,2}$) take a simplified form as $H_{\text{int}} = \frac{U}{2} \sum_{\mathbf{r}} (n_\mathbf{r}^2 - \frac{1}{3}L_{z,\mathbf{r}}^2)$, with the orbital angular momentum $L_{z,\mathbf{r}} \equiv -i(p_{x,\mathbf{r}}^\dagger p_{y,\mathbf{r}} - p_{y,\mathbf{r}}^\dagger p_{x,\mathbf{r}})$ [12].

Weak interaction limit. To understand the many-body phenomena, we first discuss the physics in the weakly interacting superfluid regime with $t_{\parallel,\perp} \gg U$ and $U_{1,2}$, where the bosons are expected to condense. For triangular lattices, the Brillouin zone forms the shape of a regular hexagon with the edge length $4\pi/3$, where the lattice constant is set to be the unit of length. The single-particle spectrum of the noninteracting p-band bosonic system is shown in Figs. 1(b) and 1(c), where we plot the dispersion of the lowest p-orbital band of a 2D triangular lattice. For $t_\perp = 0$, the system supports three degenerate minima located at $\mathbf{M}_0 = (0, 2\pi/\sqrt{3})$ and $\mathbf{M}_\pm = (\pm\pi, \pi/\sqrt{3})$ [Fig. 1(b)]. For $t_\parallel = 0$, the band minima move to the center of the Brillouin zone [Fig. 1(c)]. Due to the competition between hopping $t_\parallel$ and $t_\perp$, it is expected to develop rich orbital orders with the appearance of orbital angular momentum $\langle L_{z,\mathbf{r}} \rangle \neq 0$. We find that the system supports two different types of condensates in the weakly interacting regime. The ground state in the limit of $t_\perp \ll t_\parallel$ is a stripe superfluid phase [S_{SF} phase in Fig. 1(d)], which is described by

$$
\Phi_N^1 \propto \left[\sum_{\mathbf{r}} e^{i(\mathbf{k}\cdot\mathbf{r}+\beta_\mathbf{r})} (\cos\alpha\, p_{x,\mathbf{r}}^\dagger \pm i\sigma_\mathbf{r}\sin\alpha\, p_{y,\mathbf{r}}^\dagger) \right]^N |0\rangle. \quad (2)
$$

In the regime of $t_\parallel \ll t_\perp$, the system condenses at the center of the Brillouin zone and demonstrates a ferroorbital order [H_{SF} phase in Fig. 1(d)], with

$$
\Phi_N^2 \propto \left[\sum_{\mathbf{r}} e^{i\mathbf{k}\cdot\mathbf{r}} (p_{x,\mathbf{r}}^\dagger \pm i p_{y,\mathbf{r}}^\dagger) \right]^N |0\rangle. \quad (3)
$$

Here, $|0\rangle$ is the vacuum state, N denotes the total number of particles, $\sigma_\mathbf{r} = \pm 1$ is the sign of the staggered orbital angular momentum, $\beta_\mathbf{r} = 0$ ($\sigma_\mathbf{r} = 1$) or $\pi/2$ ($\sigma_\mathbf{r} = -1$) in the stripe direction, and $\beta_\mathbf{r} = \pi$ in the homogeneous direction. Note here that $\alpha = \pi/6$ in the regime of $t_\parallel \gg t_\perp$ and $t_{\parallel,\perp}/U \gg 1$ [30] and the bosons condense at two of the three degenerate minima as observed in the experiments [17], which is consistent with our numerical simulations.

Orbital skyrmion lattice state at strong interaction. Considering the tunability of Hubbard parameters experimentally [11], we extend our study to the strongly interacting regime of the spinless p-orbital bosons in the triangular lattice, described by Eq. (1). To analyze quantum ground states of the many-body system, a bosonic version of dynamical mean-field theory is implemented. We remark here that BDMFT is an extension of fermionic dynamical mean-field theory, and suitable to treat strongly correlated systems for the full range of couplings from Mott insulator to superfluid. To accommodate long-range orders that spontaneously break lattice-translational symmetry, we generalize a real-space BDMFT [31] for our system of spinless p-orbital bosons in the triangular lattice. The technical details can be found in the Supplementary Materials [32].

At strong interactions, bosons form a Mott-insulating state. Through BDMFT calculation, we find this Mott state develops spontaneous orbital polarization forming a skyrmion lattice that breaks time-reversal and lattice-translational symmetries. Interestingly, the BDMFT calculation reveals two different types of commensurate skyrmion textures [33–36], i.e., skyrmion and anti-skyrmion lattices as shown in Fig. 1(e), where an orbital polarization vector $\langle \boldsymbol{\mathcal{S}}_{\mathbf{r}} \rangle = (\langle \mathcal{S}_{\mathbf{r}}^x \rangle, \langle \mathcal{S}_{\mathbf{r}}^y \rangle, \langle \mathcal{S}_{\mathbf{r}}^z \rangle)$ is defined, with $\mathcal{S}_{\mathbf{r}}^x \equiv \frac{1}{2}(p_{x,\mathbf{r}}^\dagger p_{x,\mathbf{r}} - p_{y,\mathbf{r}}^\dagger p_{y,\mathbf{r}})$, $\mathcal{S}_{\mathbf{r}}^y \equiv \frac{1}{2}(p_{x,\mathbf{r}}^\dagger p_{y,\mathbf{r}} + p_{y,\mathbf{r}}^\dagger p_{x,\mathbf{r}})$, and $\mathcal{S}_{\mathbf{r}}^z \equiv \frac{1}{2i}(p_{x,\mathbf{r}}^\dagger p_{y,\mathbf{r}} - p_{y,\mathbf{r}}^\dagger p_{x,\mathbf{r}})$. The two skyrmion lattice phases are connected by the $\mathcal{T} \times \mathcal{I}$ symmetry, with $\mathcal{T}$ and $\mathcal{I}$ being time-reversal and space-reflection ($p_{x,\mathbf{r}} \to -p_{x,\mathbf{r}}$) symmetries, respectively. By mapping the real-space skyrmion onto the Bloch sphere and calculating the topological charge, this skyrmion phase reminisces a fractional skyrmion [25], as shown by the zoom of Fig. 1(e). We remark here that the emergent orbital skyrmion texture observed here is solely induced by onsite interactions, and the underlying physics is the interplay of p-orbital symmetry and geometric frustration of the triangular lattice, captured by an effective orbital-exchange model (this model will be discussed later).

To show the robustness of skyrmion texture against quantum fluctuations, we map out the full $t_\parallel - t_\perp$ phase diagram for filling $n_{\mathbf{r}} = 1$ and interactions $U = 3U_1 = 3U_2$ in the framework of BDMFT, as shown in Fig. 1(d). We find that the orbital skyrmion lattice is robust against quantum fluctuations and explores a wide regime in Mott phases. Only for sufficiently large asymmetry between the two hopping amplitudes, two other Mott phases develop instead, including stripe-orbital phase (S_{MI}) breaking time-reversal symmetry, and ferroorbital phase (H_{MI}) respecting time-reversal symmetry (real-space orbital textures shown in Fig. S1 [32]). All of these orbital-ordered phases are found to persist up to the superfluid transition. After the Mott-superfluid transition, the system demonstrates two superfluid phases, where one is a stripe-orbital phase (S_{SF}) breaking time-reversal, lattice-translational and rotational symmetries [30], and the other a ferroorbital phase (H_{SF}) breaking time-reversal symmetry, consistent with Eqs. (2) and (3). Note here that the phase diagram is symmetric upon orbital interchange in the low-hopping regime, which is also manifested in the effective orbital-exchange model [Eq. (4)].

To quantify phase boundaries in Fig. 1(d), we introduce the condensate density $\phi_\nu \equiv \sum_{\mathbf{r}} |\langle p_{\nu,\mathbf{r}} \rangle|/N_{\text{lat}}$, stripe order $\Theta_{\text{stripe}} \equiv \frac{1}{2}(\langle \mathcal{S}_+^z \rangle - \langle \mathcal{S}_-^z \rangle)$, lattice version of topological charge Q [24,26,37,38], and scalar spin chirality $\chi = \frac{1}{N_{\text{lat}}} \sum_{\mathbf{r}} \langle \frac{\boldsymbol{\mathcal{S}}_{\mathbf{r}}}{|\boldsymbol{\mathcal{S}}_{\mathbf{r}}|} \cdot (\frac{\boldsymbol{\mathcal{S}}_{\mathbf{r}+\mathbf{e}_1}}{|\boldsymbol{\mathcal{S}}_{\mathbf{r}+\mathbf{e}_1}|} \times \frac{\boldsymbol{\mathcal{S}}_{\mathbf{r}+\mathbf{e}_2}}{|\boldsymbol{\mathcal{S}}_{\mathbf{r}+\mathbf{e}_2}|}) \rangle$, where N_{lat} is the number of lattice sites and $\langle \mathcal{S}_+^z \rangle$ ($\langle \mathcal{S}_-^z \rangle$) denotes the z-component of the orbital polarization per site on the stripe with positive (negative) value. We clearly observe nonzero values of scalar spin chirality $\chi \neq 0$ and topological charge $Q \neq 0$ in the skyrmion phase, as shown in Fig. 2(a). For larger hopping amplitudes, we find a Mott phase transition from the skyrmion to the S_{MI} phase, indicated by the absence of χ, $Q = 0$ and the appearance of $\Theta_{\text{stripe}} \neq 0$. The corresponding contour plots of static spin structure factor $\mathcal{F}^z(\boldsymbol{k}) = \sum_{i,j} e^{i\boldsymbol{k}\cdot(\mathbf{r}_i - \mathbf{r}_j)} \langle \mathcal{S}_{\mathbf{r}_i}^z \mathcal{S}_{\mathbf{r}_j}^z \rangle$ are shown in the inset of Fig. 2(a) for skyrmion phases, where i and j denote the lattice sites. By increasing the hopping ampli-
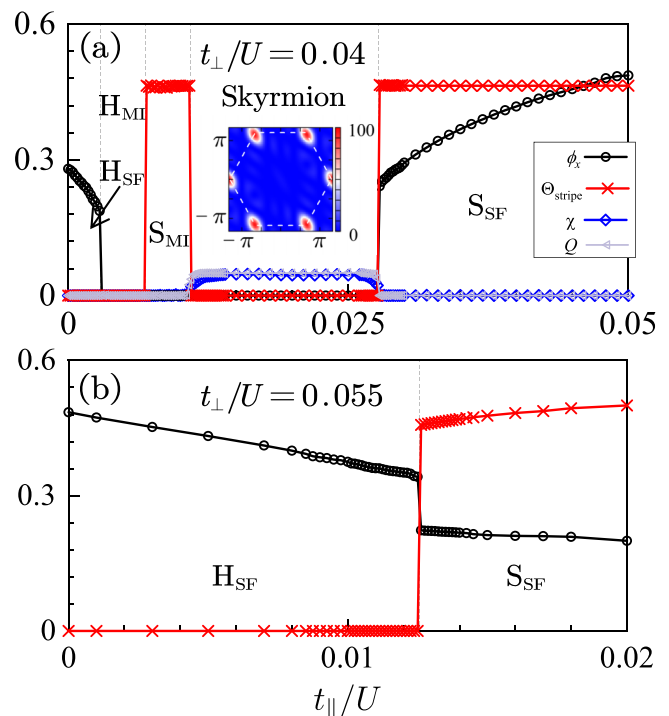

FIG. 2. Phase transitions of ultracold bosonic gases in p-orbital bands of a 2D triangular lattice for different hopping amplitudes (a) $t_\perp = 0.04U$ and (b) $t_\perp = 0.055U$, obtained via bosonic dynamical mean-field theory [32]. Indicated by the dashed lines, the system demonstrates (a) Mott transitions from the ferroorbital phase (H_{MI}) to the stripe-orbital phase (S_{MI}) and skyrmion phase, and (b) a superfluid transition from the ferro phase (H_{SF}) to a stripe phase (S_{SF}) upon small increasing hopping $t_\parallel$. Inset: Contour plots of spin structure factor $\mathcal{F}^z(\boldsymbol{k})$ for skyrmion phases. The interactions $U = 3U_1 = 3U_2$, and filling $n_{\mathbf{r}} = 1$. The other parameters for (b) are the same as those for (a).

tudes further, atoms delocalize with the coexistence of stripe order $\Theta_{\text{stripe}} \neq 0$ and superfluid order $\phi_{x,y} \neq 0$. In addition, we observe a superfluid phase transition from a ferro to a stripe-orbital order, as shown in Fig. 2(b). We remark here that the phase transitions are found to be discontinued within BDMFT.

Orbital exchange and effective model construction. To explain the underlying mechanism of the orbital textures in the deep Mott regime with $t_{\parallel,\perp} \ll U$ and unit filling, we construct an effective orbital-exchange model for Eq. (1). In our case, the orbital-exchange interactions arise from the virtual hopping processes induced by $t_{\parallel,\perp}$, and are obtained from the perturbative expansion of tunneling processes up to third order (third-order expansion will be justified later). By introducing the projection operator $\mathcal{P}$ to describe the Hilbert space of the singly occupied Mott state, the effective Hamiltonian reads $H_{\text{eff}}\mathcal{P}|\psi\rangle = E\mathcal{P}|\psi\rangle$, where $H_{\text{eff}} = -\mathcal{P}H_t \mathcal{Q}(\mathcal{Q}H\mathcal{Q} - E)^{-1}\mathcal{Q}H_t\mathcal{P}$ with $\mathcal{Q} = 1 - \mathcal{P}$, and H_t being the hopping part of Eq. (1). Due to $E \sim t^2/U$, we obtain $\mathcal{Q}H\mathcal{Q} - E \approx \mathcal{Q}H\mathcal{Q}$.

Generally, the orbital polarization operator $\boldsymbol{\mathcal{S}}_{\mathbf{r}}$ changes with bond orientations [30,39–41]. It is convenient to introduce the rotation direction $\mathbf{e}_\theta$ for orbital polarization operator, i.e., $\mathbf{e}_\theta^x = \cos(2\theta)\mathbf{e}_x + \sin(2\theta)\mathbf{e}_y$, $\mathbf{e}_\theta^y = -\sin(2\theta)\mathbf{e}_x + \cos(2\theta)\mathbf{e}_y$ and $\mathbf{e}_\theta^z = \mathbf{e}_z$, for a bond directing at angle θ with the x axis. With the definition above,
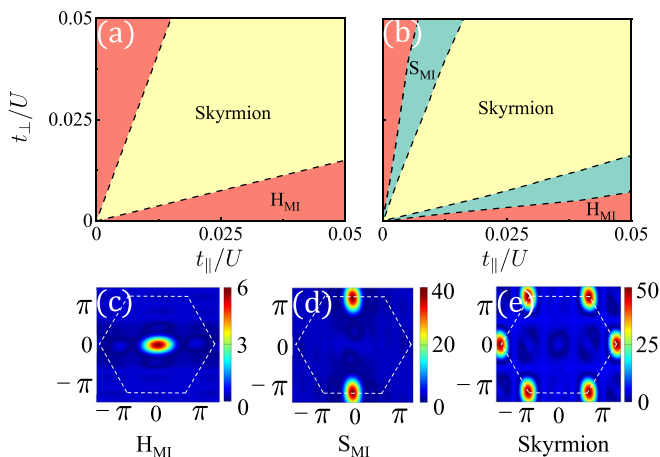
FIG. 3. Phase diagrams of (a) second- and (b) third-order anisotropic orbital-exchange models as a function of hopping amplitudes $t_\parallel$ and $t_\perp$, obtained from exact diagonalizations for a lattice of $N_{lat} = 24$ sites [32]. The effective model with third-order exchange interactions favors three Mott-insulating phases with skyrmion, stripe (S_{MI}), and ferroorbital (H_{MI}) textures, consistent with BDMFT results. (c)–(e) Contour plots of spin structure factor $\mathcal{F}^z(\mathbf{k})$ for different Mott phases. The interactions are $U = 3U_1 = 3U_2$.

FIG. 4. (a) Low-energy spectra E_i, scalar spin chirality χ, and topological charge Q as a function of $t_\perp/U$, obtained from exact diagonalizations, where the blue dots denote the ground-state degeneracy and the gray squares are for the excited states. ED calculations of real-space (b) skyrmion and (c) anti-skyrmion orbital textures [32], where the arrows represent the projection in the xy-plane of orbital polarization texture $\langle \mathcal{S}_\mathbf{r} \rangle$, and the color denotes the z component. Here, $t_\parallel/U \equiv 0.01$, $U = 3U_1 = 3U_2$, and the lattice size $N_{lat} = 3 \times 6$.

we finally obtain an anisotropic orbital-exchange model for the triangular lattice system with interactions $U = 3U_1 = 3U_2$ [32],

$$
\begin{aligned}
H_{\text{eff}} &= \sum_{\mathbf{r},m,v} (J_v + J_v') \big[\mathcal{S}_\mathbf{r} \cdot \mathbf{e}_{\theta_m}^v \big] \big[\mathcal{S}_{\mathbf{r}+\mathbf{e}_m} \cdot \mathbf{e}_{\theta_m}^v \big] \\
&\quad + \sum_{\mathbf{r},u,v,w} J_{uvw}' \big[\mathcal{S}_\mathbf{r} \cdot \mathbf{e}_{\theta_1}^u \big] \big[\mathcal{S}_{\mathbf{r}+\mathbf{e}_1} \cdot \mathbf{e}_{\theta_1}^v \big] \big[\mathcal{S}_{\mathbf{r}+\mathbf{e}_2} \cdot \mathbf{e}_{\theta_1}^w \big], \quad (4)
\end{aligned}
$$

where $\{u, v, w\} = \{x, y, z\}$, θ_m is the angle with the x axis for the bond $\mathbf{e}_m$, and J and J' denote the orbital-exchange terms from second- $\mathcal{O}(t_{\parallel,\perp}^2/U)$ and third-order $\mathcal{O}(t_{\parallel,\perp}^3/U^2)$ tunneling processes, respectively. In the absence of third-order interactions, the effective model reduces to an XYZ model with orbital-exchange parameters $J_x = -3(t_\parallel^2 + t_\perp^2)/2U$, $J_y = 3t_\parallel t_\perp/U$, and $J_z = 9t_\parallel t_\perp/U$ [16]. Generally, J_x dominates in the regime of $t_\perp \ll t_\parallel$ or $t_\parallel \ll t_\perp$, where in-plane ferroorbital order develops, and J_z dominates the remains ($t_\parallel \approx t_\perp$), where the system favors out-of-plane Ising-orbital order for bipartite lattices. For triangular lattices, however, the exchange coupling J_z ($t_\parallel \approx t_\perp$) results in Ising-type frustration [42–46] forming novel quantum phases [45,47]. In addition, the orbital-exchange interactions in Eq. (4) are strongly anisotropic, as a result of the anisotropic p-orbital hopping, leading to unique properties in the triangular lattice, as shown below.

We numerically solve the frustrated orbital-exchange model by ED with QUSPIN PYTHON package [48,49]. Here, we mainly consider lattices with periodic boundary conditions [32]. Phase diagrams of the orbital-exchange model are shown in Figs. 3(a) and 3(b). Here, it is important to note that the phase diagram of BDMFT is based on a system size of 24×24 with an ED performed on 24 sites. The disagreement of phase boundaries of Figs. 1(d) and 3 is attributed to finite-size effects. To distinguish different Mott-insulating
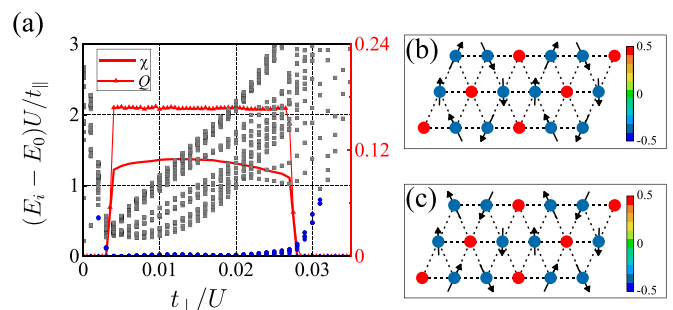
phases, both fidelity metric g (Fig. S4 [32]) [50–52] and static spin structure factor $\mathcal{F}^z(\mathbf{k})$ are utilized. Within ED, we find that the orbital skyrmion phase is described by the effective orbital-exchange model with leading-order $\mathcal{O}(t_{\parallel,\perp}^2/U)$ tunneling processes, as shown in Fig. 3(a). Considering the absence of Dzyaloshinskii-Moriya interactions [19–23] in the effective model, the mechanism for generating orbital skyrmion texture is a result of the interplay of hopping-induced anisotropic orbital-exchange interactions and geometric frustration of the triangular lattice. The leading-order orbital-exchange model, however, only favors two Mott phases, i.e., skyrmion and H_{MI} [Fig. 3(a)]. After including subleading-order $\mathcal{O}(t_{\parallel,\perp}^3/U^2)$ tunneling processes, ED resolves three Mott phases, i.e., skyrmion, S_{MI} and H_{MI} [Fig. 3(b)], whose conclusion is consistent with the prediction of BDMFT for the extended Bose-Hubbard model [Fig. 1(d)]. The corresponding static spin structure factors $\mathcal{F}^z(\mathbf{k})$ for each phase are shown in Figs. 3(c) to 3(e) [consistent with the inset of Fig. 2(a), obtained from BDMFT]. We remark here that subleading-order orbital-exchange interactions are absent in the previous studies [30,39–41] and should be included in the effective model to obtain the complete Mott phases.

To obtain more insights of the skyrmion phases, we investigate ground-state degeneracy, scalar spin chirality χ, topological charge Q, and real-space orbital textures. As shown in Fig. 4(a), we find that the skyrmion phase is actually a gapped phase with a ground-state degeneracy and displays a finite scalar spin chirality order $\chi \neq 0$ and topological charge $Q \neq 0$ [32], where both the degeneracy, χ and Q disappear in the other two Mott phases. We remark here that one only expects an approximate degeneracy in simulations due to finite-size effects. The ground-state degeneracy indicates the possibility of different types of orbital skyrmion textures. As shown in Figs. 4(b) and 4(c), two different types of real-space orbital textures are resolved within ED [32]. This prediction is consistent with BDMFT results [Fig. 1(e)]. In addition, we also calculate orbital correlations between different lattice sites for the skyrmion phase, and observe

long-range correlations for the three components of the orbital polarization [32].

Experimental detection. One key feature of the orbital skyrmion lattice phase is the momentum structure shown in Figs. 2 and 3. Its spin analog has been revealed by neutron scattering experiments [22]. The momentum structure of the orbital skyrmion lattice state can be probed by combining interorbital transition techniques [3,53] and Bragg spectroscopy [54]. With the interorbital transition techniques [53], which has been demonstrated in experiments [3], the orbital texture can be converted to density modulations, which maintain the same crystal structure. The periodic density modulations can then be probed by the standard Bragg spectroscopy in cold atom experiments [54].

Conclusion. We study cold atoms loaded in the p-orbital band of a triangular optical lattice and find a chiral orbital skyrmion lattice phase in a large part of the phase diagram. This quantum state emerges due to natural anisotropic orbital-exchange interaction for p-orbital bosons, unlike the conventional Dzyaloshinskii-Moriya scenario. In this multiorbital setting, the skyrmion and anti-skyrmion lattice states are exactly degenerate due to time-reversal symmetry, in contrast to the widely studied skyrmion lattice states in spin systems. The exotic orbital polarization texture of the orbital skyrmion state can be probed by Bragg spectroscopy, a technique accessible to most cold atom experiments.

[1] L. Niu, S. Jin, X. Chen, X. Li, and X. Zhou, Observation of a dynamical sliding phase superfluid with p-band bosons, Phys. Rev. Lett. **121**, 265301 (2018).

[2] S. Jin, W. Zhang, X. Guo, X. Chen, X. Zhou, and X. Li, Evidence of potts-nematic superfluidity in a hexagonal sp^2 optical lattice, Phys. Rev. Lett. **126**, 035301 (2021).

[3] H. Shui, S. Jin, Z. Li, F. Wei, X. Chen, X. Li, and X. Zhou, Atom-orbital qubit under nonadiabatic holonomic quantum control, Phys. Rev. A **104**, L060601 (2021).

[4] X.-Q. Wang, G.-Q. Luo, J.-Y. Liu, W. V. Liu, A. Hemmerich, and Z.-F. Xu, Evidence for an atomic chiral superfluid with topological excitations, Nature (London) **596**, 227 (2021).

[5] B. Song, S. Dutta, S. Bhave, J.-C. Yu, E. Carter, N. Cooper, and U. Schneider, Realizing discontinuous quantum phase transitions in a strongly correlated driven optical lattice, Nat. Phys. **18**, 259 (2022).

[6] T. Hartke, B. Oreg, N. Jia, and M. Zwierlein, Quantum register of fermion pairs, Nature (London) **601**, 537 (2022).

[7] M. Mamaev, P. He, T. Bilitewski, V. Venu, J. H. Thywissen, and A. M. Rey, Collective p-wave orbital dynamics of ultracold fermions, Phys. Rev. Lett. **127**, 143401 (2021).

[8] M. Hachmann, Y. Kiefer, J. Riebesehl, R. Eichberger, and A. Hemmerich, Quantum degenerate fermi gas in an orbital optical lattice, Phys. Rev. Lett. **127**, 033201 (2021).

[9] V. Venu, P. Xu, M. Mamaev, F. Corapi, T. Bilitewski, J. P. D'Incao, C. J. Fujiwara, A. M. Rey, and J. H. Thywissen, Unitary p-wave interactions between fermions in an optical lattice, Nature (London) **613**, 262 (2023).

[10] M. N. Kosch, L. Asteria, H. P. Zahn, K. Sengstock, and C. Weitenberg, Multifrequency optical lattice for dynamic lattice-geometry control, Phys. Rev. Res. **4**, 043083 (2022).

[11] G. Wirth, M. Ölschläger, and A. Hemmerich, Evidence for orbital superfluidity in the p-band of a bipartite optical square lattice, Nat. Phys. **7**, 147 (2011).

[12] W. V. Liu and C. Wu, Atomic matter of nonzero-momentum Bose-Einstein condensation and orbital current order, Phys. Rev. A **74**, 013607 (2006).

[13] A. B. Kuklov, Unconventional strongly interacting Bose-Einstein condensates in optical lattices, Phys. Rev. Lett. **97**, 110405 (2006).

[14] L.-K. Lim, C. M. Smith, and A. Hemmerich, Staggered-vortex superfluid of ultracold bosons in an optical lattice, Phys. Rev. Lett. **100**, 130402 (2008).

[15] X. Li, Z. Zhang, and W. V. Liu, Time-reversal symmetry breaking of p-orbital bosons in a one-dimensional optical lattice, Phys. Rev. Lett. **108**, 175302 (2012).

[16] X. Li and W. V. Liu, Physics of higher orbital bands in optical lattices: A review, Rep. Prog. Phys. **79**, 116401 (2016).

[17] X.-Q. Wang, G.-Q. Luo, J.-Y. Liu, G.-H. Huang, Z.-X. Li, C. Wu, A. Hemmerich, and Z.-F. Xu, Observation of nematic orbital superfluidity in a triangular optical lattice, arXiv:2211.05578.

[18] C. Wu, Unconventional Bose-Einstein condensations beyond the "no-node" theorem, Mod. Phys. Lett. B **23**, 1 (2009).

[19] U. K. Rößler, A. N. Bogdanov, and C. Pfleiderer, Spontaneous skyrmion ground states in magnetic metals, Nature (London) **442**, 797 (2006).

[20] I. Dzyaloshinsky, A thermodynamic theory of weak ferromagnetism of antiferromagnetics, J. Phys. Chem. Solids **4**, 241 (1958).

[21] T. Moriya, Anisotropic superexchange interaction and weak ferromagnetism, Phys. Rev. **120**, 91 (1960).

[22] S. Muehlbauer, B. Binz, F. Jonietz, C. Pfleiderer, A. Rosch, A. Neubauer, R. Georgii, and P. Boeni, Skyrmion lattice in a chiral magnet, Science **323**, 915 (2009).

[23] X. Yu, Y. Onose, N. Kanazawa, J. H. Park, J. Han, Y. Matsui, N. Nagaosa, and Y. Tokura, Real-space observation of a two-dimensional skyrmion crystal, Nature (London) **465**, 901 (2010).

[24] D. Amoroso, P. Barone, and S. Picozzi, Spontaneous skyrmionic lattice from anisotropic symmetric exchange in a ni-halide monolayer, Nat. Commun. **11**, 5784 (2020).

[25] S. Gao, H. Rosales, F. A. Gómez Albarracín, V. Tsurkan, G. Kaur, T. Fennell, P. Steffens, M. Boehm, P. Čermák, A.

Schneidewind *et al.*, Fractional antiferromagnetic skyrmion lattice induced by anisotropic couplings, Nature (London) **586**, 37 (2020).

[26] T. Okubo, S. Chung, and H. Kawamura, Multiple-q states and the skyrmion lattice of the triangular-lattice Heisenberg antiferromagnet under magnetic fields, Phys. Rev. Lett. **108**, 017206 (2012).

[27] M. Mohylna, F. A. Gómez Albarracín, M. Žukovič, and H. D. Rosales, Spontaneous antiferromagnetic skyrmion/antiskyrmion lattice and spiral spin-liquid states in the frustrated triangular lattice, Phys. Rev. B **106**, 224406 (2022).

[28] A. Leonov and M. Mostovoy, Multiply periodic states and isolated skyrmions in an anisotropic frustrated magnet, Nat. Commun. **6**, 8275 (2015).

[29] T. Shimokawa, T. Okubo, and H. Kawamura, Multiple-q states of the $J_1 - J_2$ classical honeycomb-lattice Heisenberg antiferromagnet under a magnetic field, Phys. Rev. B **100**, 224404 (2019).

[30] C. Wu, W. V. Liu, J. Moore, and S. Das Sarma, Quantum stripe ordering in optical lattices, Phys. Rev. Lett. **97**, 190406 (2006).

[31] Y. Li, M. R. Bakhtiari, L. He, and W. Hofstetter, Tunable anisotropic magnetism in trapped two-component Bose gases, Phys. Rev. B **84**, 144411 (2011).

[32] See Supplemental Material at http://link.aps.org/supplemental/10.1103/PhysRevResearch.5.L042042 for additional details about the method, real-space orbital texture, filling-dependent phase diagram, effective orbital exchange model, finite-size clusters in ED, fidelity metric, and real-space orbital correlations which includes Refs. [25,30,31,34,39,40,50–52,55–73].

[33] W. S. Cole, S. Zhang, A. Paramekanti, and N. Trivedi, Bose-Hubbard models with synthetic spin-orbit coupling: Mott insulators, spin textures, and superfluidity, Phys. Rev. Lett. **109**, 085302 (2012).

[34] L. He, A. Ji, and W. Hofstetter, Bose-Bose mixtures with synthetic spin-orbit coupling in optical lattices, Phys. Rev. A **92**, 023630 (2015).

[35] F. Sun, J. Ye, and W.-M. Liu, Quantum incommensurate skyrmion crystals and commensurate to in-commensurate transitions in cold atoms and materials with spin–orbit couplings in a Zeeman field, New J. Phys. **19**, 083015 (2017).

[36] K. Hejazi, Z.-X. Luo, and L. Balents, Heterobilayer moiré magnets: Moiré skyrmions and commensurate-incommensurate transitions, Phys. Rev. B **104**, L100406 (2021).

[37] B. Berg and M. Lüscher, Definition and statistical distributions of a topological number in the lattice O(3) σ-model, Nucl. Phys. B **190**, 412 (1981).

[38] G. Yin, Y. Li, L. Kong, R. K. Lake, C. L. Chien, and J. Zang, Topological charge analysis of ultrafast single skyrmion creation, Phys. Rev. B **93**, 174403 (2016).

[39] E. Zhao and W. V. Liu, Orbital order in Mott insulators of spinless p-band fermions, Phys. Rev. Lett. **100**, 160403 (2008).

[40] C. Wu, Orbital ordering and frustration of p-band Mott insulators, Phys. Rev. Lett. **100**, 200406 (2008).

[41] H. Chen and X. C. Xie, Orbital order in a bosonic p-band triangular lattice, Phys. Rev. B **103**, 205144 (2021).

[42] G. H. Wannier, Antiferromagnetism. The triangular Ising net, Phys. Rev. **79**, 357 (1950).

[43] G. Toulouse, Theory of the frustration effect in spin glasses: I, *Spin Glass Theory and Beyond*, Vol. 9 (World Scientific, 1986), pp. 99–103.

[44] R. Moessner and A. P. Ramirez, Geometrical frustration, Phys. Today **59**, 24 (2006).

[45] C. Nisoli, R. Moessner, and P. Schiffer, Colloquium: Artificial spin ice: Designing and imaging magnetic frustration, Rev. Mod. Phys. **85**, 1473 (2013).

[46] L. He, Y. Li, E. Altman, and W. Hofstetter, Quantum phases of Bose-Bose mixtures on a triangular lattice, Phys. Rev. A **86**, 043620 (2012).

[47] L. Balents, Spin liquids in frustrated magnets, Nature (London) **464**, 199 (2010).

[48] P. Weinberg and M. Bukov, Quspin: A python package for dynamics and exact diagonalisation of quantum many body systems part I: Spin chains, SciPost Phys. **2**, 003 (2017).

[49] P. Weinberg and M. Bukov, QUSPIN: A PYTHON package for dynamics and exact diagonalisation of quantum many body systems. part ii: bosons, fermions and higher spins, SciPost Phys. **7**, 020 (2019).

[50] S.-J. Gu, Fidelity approach to quantum phase transitions, Int. J. Mod. Phys. B **24**, 4371 (2010).

[51] P. Zanardi and N. Paunković, Ground state overlap and quantum phase transitions, Phys. Rev. E **74**, 031123 (2006).

[52] C. N. Varney, K. Sun, M. Rigol, and V. Galitski, Interaction effects and quantum phase transitions in topological insulators, Phys. Rev. B **82**, 115125 (2010).

[53] X. Li, A. Paramekanti, A. Hemmerich, and W. V. Liu, Proposed formation and dynamical signature of a chiral Bose liquid in an optical lattice, Nat. Commun. **5**, 3205 (2014).

[54] J. Stenger, S. Inouye, A. P. Chikkatur, D. M. Stamper-Kurn, D. E. Pritchard, and W. Ketterle, Bragg spectroscopy of a Bose-Einstein condensate, Phys. Rev. Lett. **82**, 4569 (1999).

[55] K. Byczuk and D. Vollhardt, Correlated bosons on a lattice: Dynamical mean-field theory for Bose-Einstein condensed and normal phases, Phys. Rev. B **77**, 235106 (2008).

[56] A. Hubener, M. Snoek, and W. Hofstetter, Magnetic phases of two-component ultracold bosons in an optical lattice, Phys. Rev. B **80**, 245109 (2009).

[57] P. Anders, E. Gull, L. Pollet, M. Troyer, and P. Werner, Dynamical mean field solution of the Bose-Hubbard model, Phys. Rev. Lett. **105**, 096402 (2010).

[58] Y. Li, M. R. Bakhtiari, L. He, and W. Hofstetter, Pomeranchuk effect and spin-gradient cooling of Bose-Bose mixtures in an optical lattice, Phys. Rev. A **85**, 023624 (2012).

[59] Y. Li, L. He, and W. Hofstetter, Lattice-supersolid phase of strongly correlated bosons in an optical cavity, Phys. Rev. A **87**, 051604(R) (2013).

[60] Y. Li, L. He, and W. Hofstetter, Magnetic phase transitions of spin-1 ultracold bosons in a cubic optical lattice, Phys. Rev. A **93**, 033622 (2016).

[61] Y. Li, J. Yuan, A. Hemmerich, and X. Li, Rotation-symmetry-enforced coupling of spin and angular momentum for p-orbital bosons, Phys. Rev. Lett. **121**, 093401 (2018).

[62] B. Capogrosso-Sansone, N. V. Prokof'ev, and B. V. Svistunov, Phase diagram and thermodynamics of the three-dimensional Bose-Hubbard model, Phys. Rev. B **75**, 134302 (2007).

[63] I. Vasić, A. Petrescu, K. Le Hur, and W. Hofstetter, Chiral bosonic phases on the Haldane honeycomb lattice, Phys. Rev. B **91**, 094502 (2015).

[64] K. Plekhanov, I. Vasić, A. Petrescu, R. Nirwan, G. Roux, W. Hofstetter, and K. Le Hur, Emergent chiral spin state in the Mott

phase of a bosonic Kane-Mele-Hubbard model, Phys. Rev. Lett. **120**, 157201 (2018).

[65] A. Georges, G. Kotliar, W. Krauth, and M. J. Rozenberg, Dynamical mean-field theory of strongly correlated fermion systems and the limit of infinite dimensions, Rev. Mod. Phys. **68**, 13 (1996).

[66] M. Caffarel and W. Krauth, Exact diagonalization approach to correlated fermions in infinite dimensions: Mott transition and superconductivity, Phys. Rev. Lett. **72**, 1545 (1994).

[67] F. Pinheiro, G. M. Bruun, J.-P. Martikainen, and J. Larson, *xyz* quantum Heisenberg models with *p*-orbital bosons, Phys. Rev. Lett. **111**, 205302 (2013).

[68] B. Liu, P. Zhang, H. Gao, and F. Li, Chiral orbital magnetism of *p*-orbital bosons in optical lattices, Phys. Rev. Lett. **121**, 015303 (2018).

[69] S.-Z. Lin, A. Saxena, and C. D. Batista, Skyrmion fractionalization and merons in chiral magnets with easy-plane anisotropy, Phys. Rev. B **91**, 224407 (2015).

[70] X. Yu, W. Koshibae, Y. Tokunaga, K. Shibata, Y. Taguchi, N. Nagaosa, and Y. Tokura, Transformation between meron and skyrmion topological spin textures in a chiral magnet, Nature (London) **564**, 95 (2018).

[71] A. Auerbach, *Interacting Electrons and Quantum Magnetism* (Springer, New York, 2012).

[72] F. Essler, H. Frahm, F. Göhmann, A. Klümper, and V. Korepin, *The One-Dimensional Hubbard Model* (Cambridge University Press, Cambridge, England, 2005).

[73] X. Li, E. Zhao, and W. Vincent Liu, Topological states in a ladder-like optical lattice containing ultracold atoms in higher orbital bands, Nat. Commun. **4**, 1523 (2013).